Excitation of symmetry-protected vertical modes through arrays of coaxial sub-λ apertures for THz applications

Abdelhak Dhibi[1], Souhaila Boublouh[1], Abderrahmane Belkhir[2], Abdelaziz Mezeghrane[2], Abdullah Al Abiad[1], Lucas Grosjean[1], Maria-Pilar Bernal[1], Nadège Courjal[1], Ayman Hoblos1 and Fadi I. baida[1]

[1]Institut FEMTO-ST, UMR 6174 CNRS, 25030 Besançon Cedex, France

[2]Laboratoire de Physique et Chimie Quantique, Université Mouloud Mammeri, Tizi-Ouzou, Algeria

E-mail: abdelhakplasmons@yahoo.fr

March 2024

Abstract. We numerically study the excitation of a Symmetry-Protected *Vertical* Mode (SPVM) within a specific periodic structure of coaxial apertures made in gold. The geometrical parameters are chosen to operate in the THz domain. Contrarily to classical SP modes that correspond to a mode propagating in the direction of periodicity of the structure, here the SP mode consists on the Transverse Electro Magnetic (TEM) guided mode that propagates vertically inside the coaxial aperture along the metal thickness. This feature makes the spectral properties of the excited mode less-sensitive to the spatial extension of the grating allowing thus the design of less-cumbersome devices. We demonstrate that the spectrally localized resonance corresponding to this mode is particularly sensitive to mechanical perturbation (acoustic wave for instance) of the geometry, enabling the design of highly efficient THz modulators operating at $\lambda \approx 300$ μm with a sensitivity as great as 12.4 μm/° of the tilt angle of its metal core.

1. Introduction

The important property of nano-photonic structures lies in the confinement of the electromagnetic field which enables responses to be effective enough to reproduce those of conventional components despite the small size of the active area [1]. This is generally due to the exacerbation of the linear and, above all, non-linear properties of the material used [2]. Furthermore, nano-photonics enables us to go even further, offering functionalities unattainable in the macroscopic - and sometimes even microscopic - domains such as excitation of frozen modes [3, 4] (with very large effective refractive indices), negative refraction [5, 6], optical trapping and manipulation of nanoparticles

[7, 8, 9] (molecules and cells), and extraordinary/enhanced electromagnetic transmission [10, 11, 12, 13].

In the latter field, coaxial apertures continue to be exploited in numerous physical phenomena and potential applications such as spectral filtering, artificial anisotropy, non-linear signal generation and optical trapping [14, 15, 16, 17, 18, 19, 20, 21, 22].The properties of the modes guided in these finite-length coaxial wave-guides are the key parameters for designing specific devices to suit the desired application. Nevertheless, most applications are based on the use of the fundamental cut-off mode, i.e. the TE_{11} mode, when excited at its cutoff frequency. Under these conditions of excitation, the latter presents a group velocity that tends to zero while its phase velocity tends to infinity allowing the electromagnetic density of states to grow drastically. This leads to an enhanced interaction between light and matter that exacerbates all the linear and non-linear properties of the host medium [23, 24]. Unfortunately, the TE_{11} mode can easily be excited by a linearly polarized plane wave at normal incidence (incident wave propagating along the axis of the coaxial aperture), and is therefore not protected by symmetry. As we shall see later, its spectral signature in transmission (or reflection) is so broad that it is not compatible with high-sensitivity detection or modulation. Nonetheless, it is possible to excite another mode, namely the fundamental cutoff-less **TEM** (Transverse Electro Magnetic) mode. Fortunately, its excitation requires particular conditions [25] making it protected by symmetry (here called TEM-SPVM for: Transverse Electro Magnetic - Symmetry Protected Mode) in the case of normal incidence illumination.

In general, Symmetry-Protected Modes (SPMs) [26, 27] are considered as a variety of optical Bound states In the Continuum (BICs)[28, 29] whose symmetry properties (geometry and/or illumination) can easily explain the generation of two or more eigenmodes of the structure that will interfere destructively, leading to a resonance with a quality factor that tends towards infinity (no signature in the spectral response). A simple break in intrinsic or extrinsic symmetry can then lead to the emergence of this resonance. In the case of the coaxial structure, once excited, TEM propagation takes place within each individual aperture, making its excitation independent of the number or arrangement of apertures. The result is a spectral signature in the form of a resonance with the same quality factor whatever the overall size of the aperture matrix. This was demonstrated in reference [30] where it was shown that a single coaxial aperture exhibited the same transmission resonance as an infinitely periodic grating, apart from the transmission efficiency which is, obviously, lower. Here, we exploit this TEM-SPVM to excite it under normal incidence by introducing an extrinsic symmetry break produced by an acoustic wave vibrating the metal core of the coaxial apertures. This results in excitation of the TEM mode with a spectral signature corresponding to a resonance peak or dip, whose quality factor is all the greater the weaker the symmetry breaking [31].

2. Proposed geometry

Consider the structure shown in figure 1. It consists of a bi-periodic array of coaxial apertures engraved into a gold film of thickness h. The inner and outer radii are R_i and R_o respectively. The gold layer is assumed to be deposited on a Teflon substrate, and the grating is illuminated from the side of the substrate whose refractive index is $n = 1.435$, corresponding to the spectral range $\lambda \in [150; 350]$ μm. The dispersion of gold is described in the numerical simulations by a Drude critical points model [32] given by Eq. 1 with the parameters of table 1.

$$\varepsilon_{\text{Au}}(\omega) = \varepsilon_\infty - \frac{\omega_p^2}{\omega^2 + i\gamma\omega} + A \times \Omega \left\{ \frac{e^{i\phi}}{\Omega - \omega - i\Gamma} - \frac{e^{-i\phi}}{\Omega + \omega + i\Gamma} \right\} \tag{1}$$

Table 1. Parameters of the used Drude critical point dispersion model used for gold in the spectral range $\lambda \in [150; 350]\mu$m.

ε_∞	γ/π(THz)	ω_p/π (THz)	Ω/π (THz)	Γ/π (THz)	A	ϕ (rad)
1	3.848	2046.5734	2.023	3.7688	1.8021×10^5	-0.785

The transmission coefficient of such a grating is generally governed by a Fabry-Perot type law [11]. For the TEM mode which is without cutoff, the transmission maxima are located at wavelengths λ_{res} that verify the following phase matching relation:

$$\frac{4\pi n_{\text{eff}} h}{\lambda_{\text{res}}} + \phi_1 + \phi_2 = 2m\pi \tag{2}$$

where n_{eff} is the effective index of the TEM guided mode, ϕ_1 and ϕ_2 are the phases of the reflection coefficient at the substrate and superstrate interfaces respectively, and m is a positive non zero integer.

This equation shows that a minimum value of thickness is required to obtain at least one transmission peak ($m = 1$ in Eq. 2) in the spectral range under consideration ($\lambda \in [150; 350]$ μm). We therefore set the thickness at $h = 100\mu$m, which will lead to a transmission peak around $\lambda = 300$ μm, as we will see later. Illumination consists of a linearly polarized plane wave propagating (vector $\vec{k}_{\text{inc}}$) in the direction given by the Euler angles θ (angle of incidence) and ψ (azimuth angle). The two polarization eigenstates TE (s) and TM (p) are defined by a third angle ϕ as shown at the bottom of figure 1a so that $\phi = 0°$ and $\phi = 90°$ correspond to the TE and TM polarization states respectively.

In order to determine the spectral position of the TEM mode, we must meet the conditions for its excitation given in ref. [25] which are: TM polarization state and oblique incidence ($\theta \neq 0$). Figure 1b shows the transmission coefficient diagrams obtained in TE polarization ($\phi = 0°$) and in TM polarization ($\phi = 90°$) as a function of the angle of incidence θ when the plan of incidence is parallel to xOy ($\psi = 0$). As expected, the excitation of the TEM-SPVM is only obtained in TM polarization and for

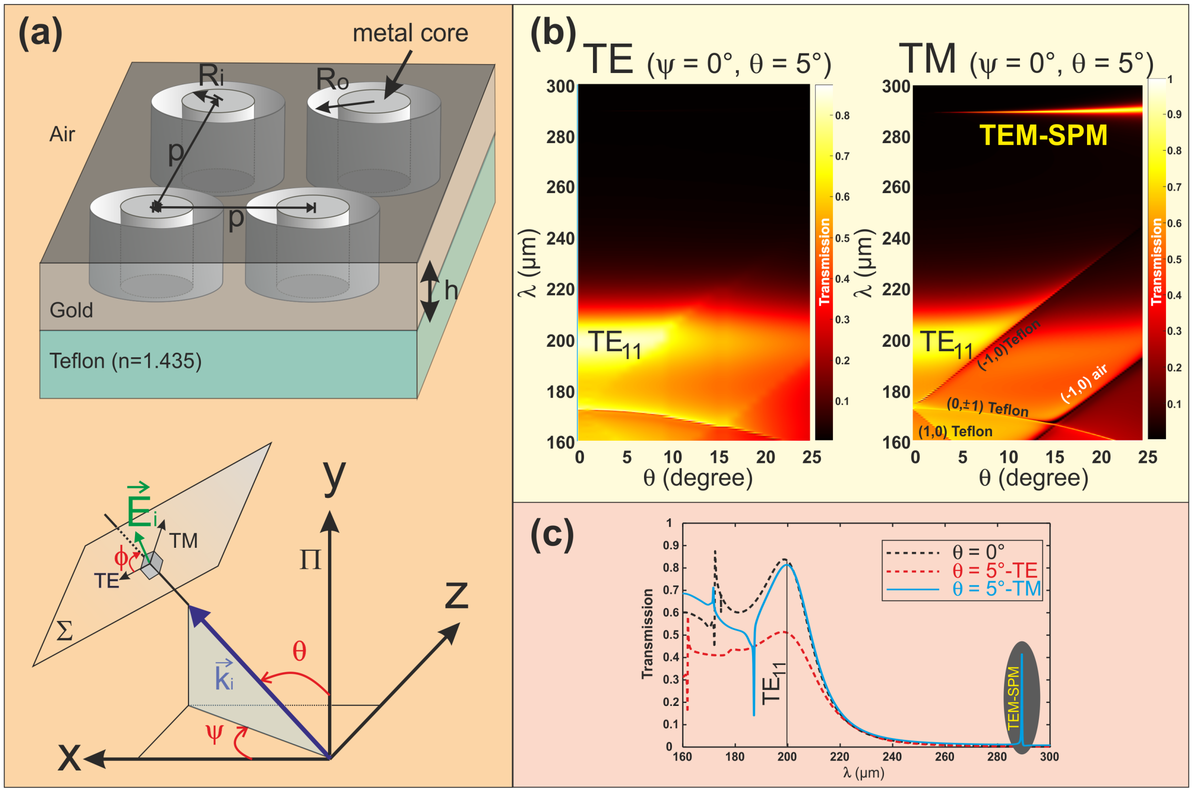

Figure 1. (a) Schematic of the proposed THz metamaterial composed of coaxial apertures arranged in a square lattice of period p. The inner and outer radii are R_i and R_o respectively. The apertures are engraved in a gold layer of thickness h that is deposited on a Teflon (PTFE) substrate. The illumination is done by a plane wave with a wavevector $\vec{k}_i$ (blue arrow) marked by the Euler angles (θ, ϕ) and incident from the substrate. Π is the plane of incidence. (b) Transmission diagram spectra as a function of the angle of incidence θ in both TE and TM polarization states ($p = 120$ μm, $R_i = 20$ μm, $R_o = 44$ μm and $h = 100$ μm). (c) Normalized transmission coefficients in TM polarization state for normal incidence $\theta = 0°$ (dashed black line) and in oblique incidence $\theta = 5°$ (dotted red lines in TE and solid blue line in TM).

$\theta \neq 0°$. The transmission peak corresponding to the first Fabry-Perot harmonic ($m = 1$ in Eq. 2) of the vertical cavity mode is located at $\lambda = 289.5$ μm. Its position can be controlled through the gold layer thickness h if necessary as underlined by Eq. 2. In addition to the wide transmission peak associated with the excitation of the TE_{11}, four lines corresponding to discontinuities appear on both TE and TM diagrams. They are more visible in TM polarization because of the large value of the normal component of the electric field amplitude (E_y) for this polarization. These discontinuities are well-known in the context of diffraction by gratings and are called the Rayleigh anomalies. They correspond to the wavelength values for which the nature of one diffracted order, in the substrate (Teflon) or in the superstrate (air), changes from radiative to evanescent. Their values are given by Eq. 1 of ref.[34]. For the considered spectral range, only 3 diffracted orders in Teflon and one in air are involved as indicated on Fig.1b for TM polarization. Figure 1c shows three transmission spectra: one (black dotted line) at normal incidence $\theta = 0°$ where both polarization states (TE,TM) are equivalent, and two calculated at oblique incidence at $\theta = 5°$, one in TE polarization (red dotted line) and one in TM polarization (blue solid line). In this last case where the two conditions of symmetry breaking and TM polarization are fulfilled, an additional transmission peak appears (gray ellipse), due to the excitation of the TEM mode, with a transmission efficiency that almost reaches 50% and with a quality factor of $Q \approx 1500$.

Otherwise, even if the experimental demonstration of the TEM mode excitation was already demonstrated in the visible range [33], the amplitude and the quality factor of the associated transmission peak were too weak to allow an efficient sensitivity to external perturbations. This is why we chose the THz range, for which noble metals such as gold are almost perfect conductors.. This is directly due to the metal losses in that spectral range that are almost 150 times larger than in THz [35].

3. Opto-mechanical results

Once we have demonstrated the possible excitation of the TEM-SPVM in oblique incidence, we study here the influence of an external perturbation on its spectral properties (position and quality factor) in the context of a mechanical perturbation. For this purpose, let consider an acoustic wave propagating along the metal layer at a given frequency that could induce the vibration of the metal cores of the coaxial apertures. After a derivation of the weak mechanical problem formulation, the FEniCS library has been chosen to support the calculation of the mechanical eigenmodes of the structure. FEniCS will enable us to solve the problem in variational finite element formulation. The NumPy library is used to manage the numerical data (eigen-frequencies and displacements) and the solution is obtained using the SLEPc library.

For the latter simulations, the Young's modulus of gold is set to $E = 77.2 \times 10^9$ Pa, the Poisson's modulus to $\nu = 0.42$ and the volume density to $\rho = 19320$ kg/m^3. Numerical simulations yield to the first bending mode's frequency to be $f = 1.05$MHz. The movie "Visualization.avi" shows the fundamental flexural mode motion of the metal core of the coaxial aperture). We can clearly see the meshing used in the FEM simulation. This mode could be excited by an interdigitated comb deposited on the Teflon interface on both sides of the coaxial aperture matrix for instance. Even if all the structure is subjected to this wave, it seems intuitive that the vibration amplitude of the cylindrical metal core will be much greater than that associated with the rest of the metal layer and especially the vertical outer cylindrical walls of the apertures. The temporal period of this megahertz acoustic wave ($T_a = 0.95$ μs) is very large compared to the time interaction delay of the THz wave with the structure estimated to be $\Delta T = \frac{\lambda_{TEM}^2}{c\Delta\lambda_{TEM}} = \frac{Q\lambda_{TEM}}{c}$. For instance, if we consider an angle of incidence $\theta = 5°$, we obtain from Fig. 1c : $\lambda_{TEM} = 289.55$ μm, $\Delta\lambda_{TEM} = 0.17$ μm and $Q \approx 1500$ leading to $\Delta T = 1.45$ ns. This means that the time needed to reach the steady state of the transmitted THz signal is almost 650 times shorter than the period of one mechanical oscillation.

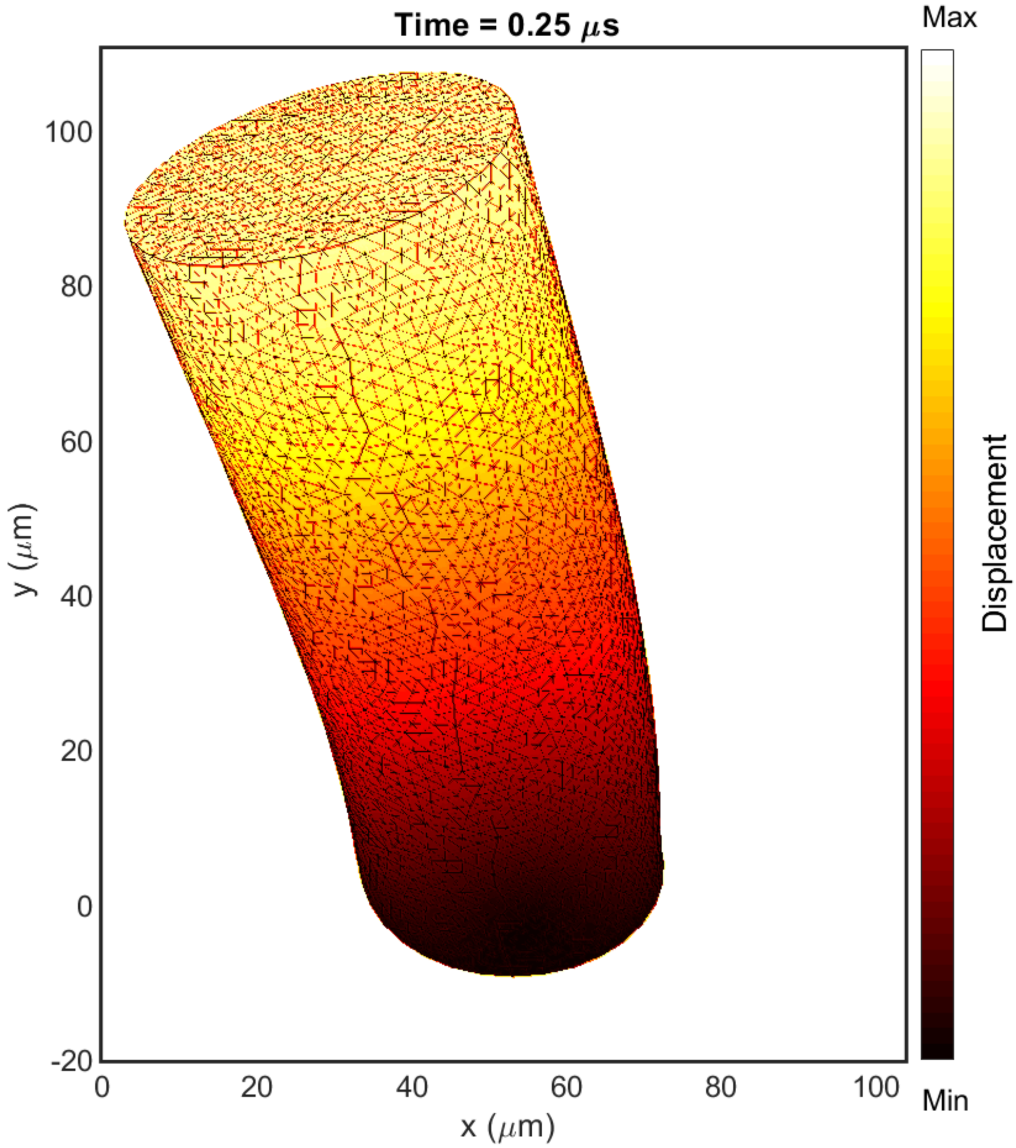

Figure 2. Illustration of the fundamental mode of vibration (bending) of the metal core of one coaxial aperture, where displacement from the initial position along the vertical axis is color-coded.

Consequently, the optical response over a bending period can be calculated by considering a quasi-static schema over the mechanical motion of the structure with enough steps fixed, in our study, to 30. To simulate this bending motion of the aperture metal core, we simply proceed by considering it to exhibit a varying angle α with the vertical direction Oy (see figure 3a). The maximum value of this angle is limited to avoid the contact with the aperture outer part. In our case, this can be controlled by the magnitude of the electrical signal feeding the interdigital comb. For our geometry, $\alpha_{max} = 12.5°$. Figure 3b shows the transmission spectra when α varies from 0 to $\alpha_{max} = 12.5°$ in both TE and TM polarization states. As expected, the TEM-SPVM

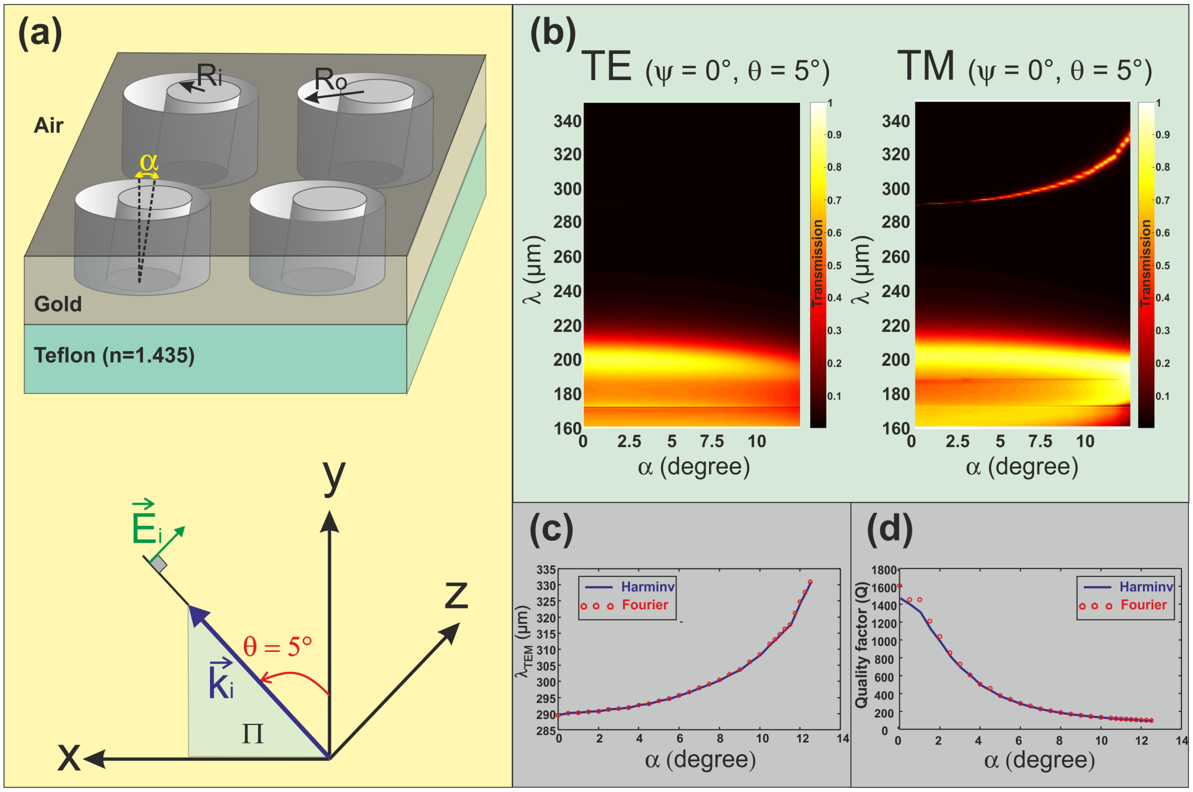

Figure 3. (a) Schematic of the vibrating coaxial apertures showing the angle of bending α located in the xy plane which is the plane of incidence Π. (b) Transmission diagram spectra as a function of the angle α varying from 0 to 12.5° in both TE and TM polarization states ($p = 150$ μm, $R_i = 20$ μm, $R_o = 44$ μm, $h = 100$ μm and $\theta = 5°$). (c) Spectral position $\lambda_{\rm TEM}$ and (d) quality factor Q of the excited TEM-SPVM as a function of α in TM polarization.

only appears in TM and its properties are very sensitive to α in terms of both spectral position (see figure 3c) and quality factor (see figure 3d), since the symmetry of the structure is more broken as α increases. Note that the Q factor was determined in two different ways: the first, called the "Fourier" value, from the TM polarization spectra of figure 3b and the second, called the "Harminv" value, using a software program called "Harminv" based on a harmonic inversion algorithm [36] often associated with FDTD simulations to extract information about highly resonant modes. Results of Fig. 3c leads to a varying value of the modulation sensitivity defined by:

$$S_{\rm m} = \frac{\Delta\lambda_{\rm TEM}}{\Delta\alpha} \quad (3)$$

At $\alpha \simeq 0°$, its value is $S_{\rm m} = 1.25$ μm/° and increases to 12.4 μm/° for α around 12°. These results demonstrate the high sensitivity of this structure to an acoustic wave tuned to the fundamental bending resonance mode of the metal core of the coaxial aperture.

To be convinced about the excitation of the TEM-SPVM, we present on Fig. 4a the electric field distribution in a vertical (xy) plane containing the axis of the aperture and in (b), the corresponding one in an horizontal (xz) plane at 2 μm from the output side (here $y = 452$ μm) in the case of $\alpha = 5°$. As expected, we can see that the first Fabry-Perot harmonic of the TEM mode is excited at this wavelength and is identified by the presence of only one electric field node (see Fig. 4a) inside the aperture and by the quasi-cylindrical symmetry of the electric field distribution given in Fig. 4b where the white arrows correspond to the transverse component of the transmitted electric field.

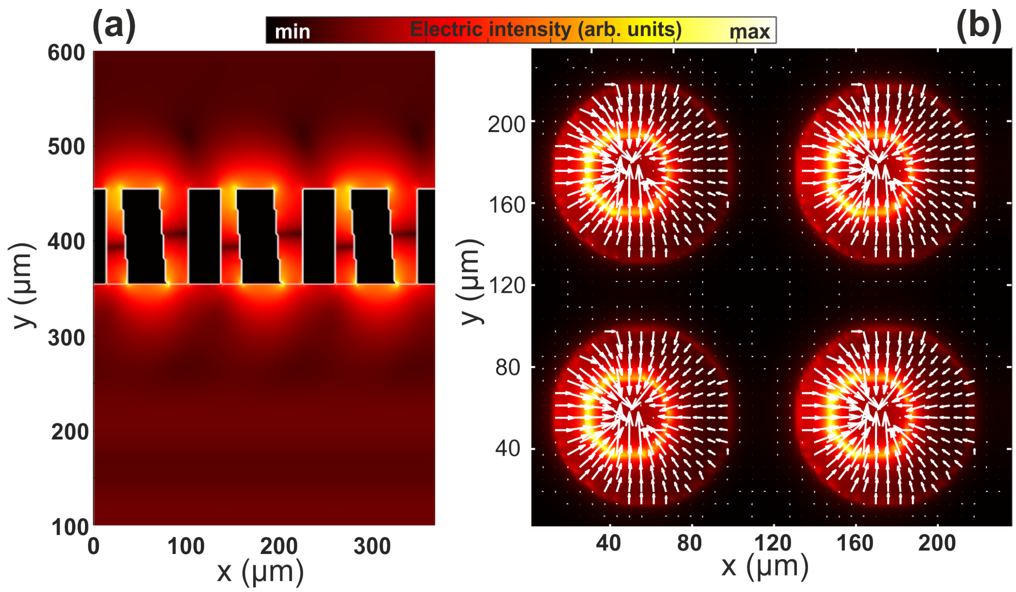

Figure 4. Electric intensity distributions in a xy vertical plane containing the axis of the apertures in (a) and in xz plane located at 2 μm for the output side in (b). The wavelength is set to $\lambda = 293.96$ μm that corresponds to the TEM-SPVM excitation at an angle of incidence $\theta = 5°$ and for a tilt angle $\alpha = 5°$.

In practice, two detection scenarios can be proposed: (1) a monochromatic time-resolved regime (instantaneous optical spectrum) where the wavelength is fixed at a value for which the TEM mode could be excited (here $\lambda \in [288; 328]$ μm) or (2) a time-average spectrum as it can be detected utilizing a slow detector such as a spectrum analyzer. An example of the THz response for each regime is given in Fig. 5 where the monochromatic regime is considered for three wavelength values (Fig. 5a) showing highly non-linear responses for which a fraction of degree is only needed to get linear modulation of the transmitted light intensity (see shaded areas on Fig. 5a that show slopes estimated to almost 0.25° for a transmission coefficient varying from 0.2 to 0.5). For the second regime, the time-average spectrum (black solid line of Fig. 5b) is calculated by integrating all the spectra of Fig. 3b in TM polarization over one THz period and it is compared to the one of the unperturbed structure ($\alpha = 0°$) in red dashed line. This demonstrate that the detection of the bending motion could be revealed even if we use a conventional un-cooled THz bolometer for which the response time is in the millisecond range.

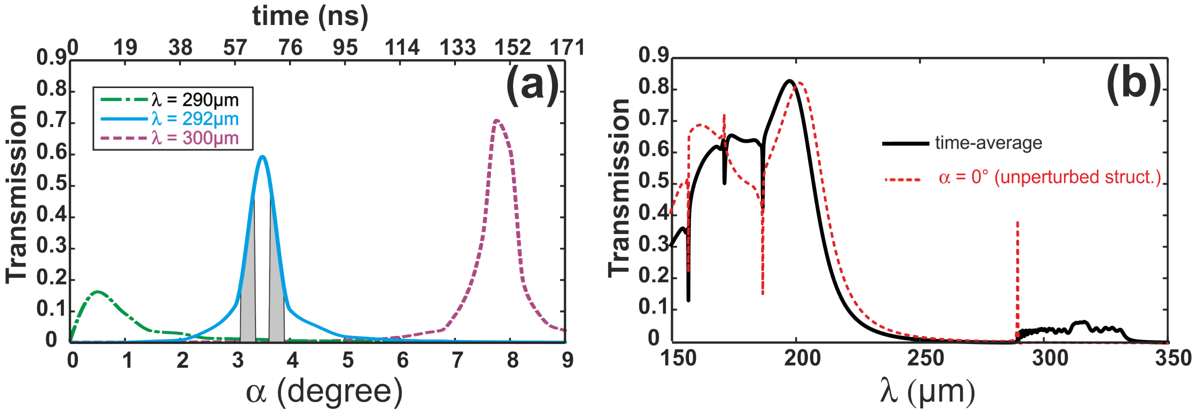

Figure 5. (a) Instantaneous THz responses as a function of time (upper horizontal axis) or bending angle α (lower horizontal axis) for three different wavelength values ($\lambda = 290$ μm in dotted-dashed green line, $\lambda = 292$ μm in solid blue line and $\lambda = 300$ μm in dotted purple line). (b) Time-average spectrum (black solid line) in comparison to the spectrum of the unperturbed structure ($\alpha = 0°$ in red dashed line). In both cases, the angle of incidence is set to $\theta = 5°$.

4. Conclusion

We demonstrate through rigorous numerical simulations that a symmetry-protected vertical mode, namely the TEM-SPVM, of a coaxial array of gold apertures can be used to modulate the intensity of the transmitted THz wave significantly, thanks to the high quality factor of its resonance and very high sensitivity to geometrical parameters. Many other applications can be envisaged, such as spectral filtering, polarization selection (only the component of the electric field parallel to the plane of vibration is transmitted) or refractive index detection in the field of biosensing. As long as the resonance properties can be controlled by the degree of symmetry breaking, it would be possible to increase the detection sensitivity or modulation efficiency of such a nano-structure while reducing the energy required to operate it.

Acknowledgments

Computations have been partially performed on the supercomputer facilities of the "Mésocentre de calcul de Franche-Comté". This work has been partially supported by the EIPHI Graduate School (contract ANR-17-EURE-0002).

Disclosures

The authors declare no conflicts of interest.

Data Availability Statement

Data underlying the results presented in this paper are not publicly available at this time but may be obtained from the authors upon reasonable request.

References

[1] T. Wu, M. Gurioli and P. Lalanne. Nanoscale Light Confinement: the Q's and V's. *ACS Photonics*, 8, 6, 1522–1538, 2021. `https://doi.org/10.1021/acsphotonics.1c00336`.

[2] J. D. Joannopoulos, S. G. Johnson , J. N. Winn and R. D. Meade. Photonic Crystals: Molding the Flow of Light - Second Edition. *Princeton: Princeton University Press*, London, 2008. `https://doi.org/10.1515/9781400828241`.

[3] A. Figotin and I. Vitebskiy. Gigantic transmission band-edge resonance in periodic stacks of anisotropic layers. *Phys. Rev. E, 72, 036619, 2005.* `https://doi.org/10.1103/PhysRevE.72.036619`.

[4] A. Figotin and I. Vitebskiy. Frozen light in photonic crystalswith degenerate band edge. *Phys. Rev. E*, 74, 066613, 2006. `https://doi.org/10.1103/PhysRevE.74.066613`.

[5] V. G. Veselago. The electrodynamics of substances with simultaneously negative values of ϵ and μ. *Soviet Physics Uspekhi*, 10, 509, 1968. `https://doi.org/10.1103/PhysRevLett.24.156`.

[6] J. B. Pendry and D. R. Smith. Reversing light with negative refraction. *Physics today*, 57(6), 37-43, 2004. `https://doi.org/10.1063/1.1784272`.

[7] A. Ashkin. Acceleration and trapping of particles by radiation pressure. *Phys. Rev. Lett.*, 24, 156, 1970. `https://doi.org/10.1103/PhysRevLett.24.156`.

[8] L. Novotny, R. X. Bian and X. S. Xie. Theory of Nanometric Optical Tweezers *Phys. Rev. Lett.* 79, 645, 1997. `https://doi.org/10.1103/PhysRevLett.79.645`.

[9] T. Shoji and T. Yasuyuki. Plasmonic optical tweezers toward molecular manipulation: tailoring plasmonic nanostructure, light source, and resonant trapping. *The journal of physical chemistry letters*, 5(17), 2957-2967, 2014. `https://doi.org/10.1021/jz501231h`.

[10] T. W. Ebbesen, H. J. Lezec, H. F. Ghaemi, T. Thio, T. andP. A. Wolff. Extraordinary optical transmission through sub-wavelength hole arrays. *Nature*, 391, 6668, 1998. `https://doi.org/10.1038/35570`.

[11] F. I. Baida and D. Van Labeke. Light transmission by subwavelength coaxial aperture arrays in metallic films. *Optics Communications*, 209, 17–22, 2002. `10.1016/S0030-4018(02)01690-5`.

[12] F. I. Baida and D. Van Labeke. Three-dimensional structures for enhanced transmission through a metallic film: Annular aperture arrays. *Phys. Rev. B*, 67, 155314, 2003. `https://doi.org/10.1103/PhysRevB.67.155314`.

[13] D. Qu and D. Grischkowsky and W. Zhang. Terahertz transmission properties of thin, subwavelength metallic hole arrays. *Opt. Lett.*, 29, 896–898, 2004. `https://doi.org/10.1364/OL.29.000896`.

[14] W. Fan and S. Zhang and B. Minhas and K. J. Malloy and S. R. J. Brueck. Enhanced Infrared Transmission through Subwavelength Coaxial Metallic Arrays. *Phys. Rev. Lett.*, 94, 033902, 2005. `https://doi.org/10.1103/PhysRevLett.94.033902`.

[15] M. I. Haftel and C. Schlockermann and G. Blumberg. Enhanced transmission with coaxial nanoapertures: Role of cylindrical surface plasmons. *Phys. Rev. B*, 74, 235405, 2006. `https://doi.org/10.1103/PhysRevB.74.235405`.

[16] F. I. Baida, A. Belkhir, D. Van Labeke and O. Lamrous. Subwavelength metallic coaxial waveguides in the optical range: Role of the plasmonic modes. *Phys. Rev. B*, 74, 205419, 2006. `https://doi.org/10.1103/PhysRevB.74.205419`.

[17] A. Agrawal and A. Nahata. Coupling terahertz radiation onto a metal wire using a subwavelength

coaxial aperture. *Opt. Express*, 15, 9022-9028, 2007. https://doi.org/10.1364/OE.15.009022.

[18] B. Vial, M. Commandré, G. Demésy, A. Nicolet, F. Zolla, F. Bedu, H. Dallaporta, S. Tisserand, and L. Roux. Transmission enhancement through square coaxial aperture arrays in metallic film: when leaky modes filter infrared light for multispectral imaging. *Opt. Lett.*, 39, 4723-4726, 2014. https://doi.org/10.1364/OL.39.004723.

[19] E. Barakat, M.-P. Bernal and F. I. Baida. Doubly resonant Ag–$LiNbO_3$ embedded coaxial nanostructure for high second-order nonlinear conversion. *J. Opt. Soc. Am. B*, 30, 1975-1980, 2013. https://doi.org/10.1364/JOSAB.30.001975.

[20] J. Lee, S. Yang, J. Lee, J.-H. Choi, Y.-H. Lee, J. H. Shin, and M.-K. Seo . Extraordinary optical transmission and second harmonic generation in sub–10-nm plasmonic coaxial aperture. *Nanophotonics*, 9, 10, 3295-3302, 2020. https://doi.org/10.1515/nanoph-2020-0066.

[21] A. A. E. Saleh and J. A. Dionne. Toward efficient optical trapping of sub-10-nm particles with coaxial plasmonic apertures. *Nano Letters*, 12, 5581-5586, 2012. https://doi.org/10.1021/nl302627c.

[22] N. Hameed, T. Zeghdoudi, B. Guichardaz, A. Mezeghrane, M. Suarez, N. Courjal, M.-P. Bernal, A. Belkhir, and F. I. Baida. Stand-alone optical spinning tweezers with tunable rotation frequency. *Opt. Express*, 31, 4379-4392, 2023. https://doi.org/10.1364/OE.480961.

[23] M. Roussey and M.-P. Bernal and N. Courjal and D. Van Labeke and F. I. Baida and R. Salut. Electro-optic effect exaltation on lithium niobate photonic crystals due to slow photons. *Appl. Phys. Lett.*, 89, 241110, 2006. https://doi.org/10.1063/1.2402946.

[24] E. Barakat, M.-P. Bernal and F. I. Baida. Theoretical analysis of enhanced nonlinear conversion from metallo-dielectric nano-structures. *Opt. Express*, 20, 16258-16268, 2012. https://doi.org/10.1364/OE.20.016258.

[25] F. I. Baida. Enhanced transmission through subwavelength metallic coaxial apertures by excitation of the TEM mode. *Appl. Phys. B*, 89, 145–149, 2007. https://doi.org/10.1007/s00340-007-2787-3.

[26] L. Lu, C. Fang, L. Fu, S. G. Johnson, J. D. Joannopoulos, and M. Soljačić. Symmetry-protected topological photonic crystal in three dimensions. *Nature Physics*, 12(4):337, 2016. https://doi.org/10.1038/nphys3611.

[27] W. Zhang, B. Gallinet and O. J. F. Martin. Symmetry and selection rules for localized surface plasmon resonances in nanostructures. *Physical Review B*, 81(23):233407, 2010. https://doi.org/10.1103/PhysRevB.81.233407.

[28] D. C. Marinica, A. G. Borisov and S. V. Shabanov. Bound states in the continuum in photonics. *Phys. Rev. Lett.*, 100, 18, 183902, 2008. https://doi.org/10.1103/PhysRevLett.100.183902.

[29] C. W. Hsu,B. Zhen, A. D. Stone, J. D. Joannopoulos and M. Soljačić. Bound states in the continuum. *Nature Reviews Materials*, 1(9), 1–13, 2016. https://DOI:10.1126/sciadv.adg47.

[30] F. I. Baida, D. Van Labeke and B. Guizal. Enhanced confined light transmission by single subwavelength apertures in metallic films. *Appl. Opt.*, 42(34), 6811-6815, 2003. https://doi.org/10.1364/AO.42.006811.

[31] Kodigala, A., Lepetit, T., Gu, Q. *et al.*. Lasing action from photonic bound states in continuum. *Nature*, 541, 196–199, 2017. https://doi.org/10.1038/nature20799.

[32] M. Hamidi, F. I. Baida, A. Belkhir and O. Lamrous. Implementation of the critical points model in a SFM-FDTD code working in oblique incidence. *Journal of Physics D: Applied Physics*, 44, 245101, 2011. https://doi.org/10.1088/0022-3727/44/24/245101.

[33] A. Ndao, A. Belkhir, L. Salut and F. I. Baida. Slanted annular aperture arrays as enhanced-transmission metamaterials: Excitation of the plasmonic transverse electromagnetic guided mode. *Appl. Phys. Lett.*, 103, 211901, 2013. https://doi.org/10.1063/1.4832227.

[34] A. Ndao and R. Salut and M. Suarez and F. I. Baida. Plasmonless polarization-selective metasurfaces in the visible range. *J. Opt.*, 20, 045003, 2014. 10.1088/2040-8986/aab1eb

[35] For gold, the skin depth at $\lambda = 250$ μm is about 40 nm ($\frac{\lambda}{40}$) while it value is of 15 nm at $\lambda = 600$ nm

$(\frac{\lambda}{6250})$.
[36] V. A. Mandelshtam and H. S. Taylor. Harmonic inversion of time signals and its applications. *J. Chem. Phys.*, 107, 6756, 1997. https://doi.org/10.1063/1.475324.